

Supplementary Materials

Modification of NiSe₂ Nanoparticles by ZIF-8-Derived NC for Boosting H₂O₂ Production from Electrochemical Oxygen Reduction in Acidic Media

Qiaoting Cheng, Hu Ding, Lang Chen, Jiatong Dong, Hao Yu, Shen Yan and Hua Wang *

Key Laboratory for Green Chemical Technology of Ministry of Education,
Collaborative Innovation Center of Chemical Science and Engineering, School of
Chemical Engineering and Technology, Tianjin University,
Tianjin 300072, China

* Correspondence: tjuwanghua@tju.edu.cn

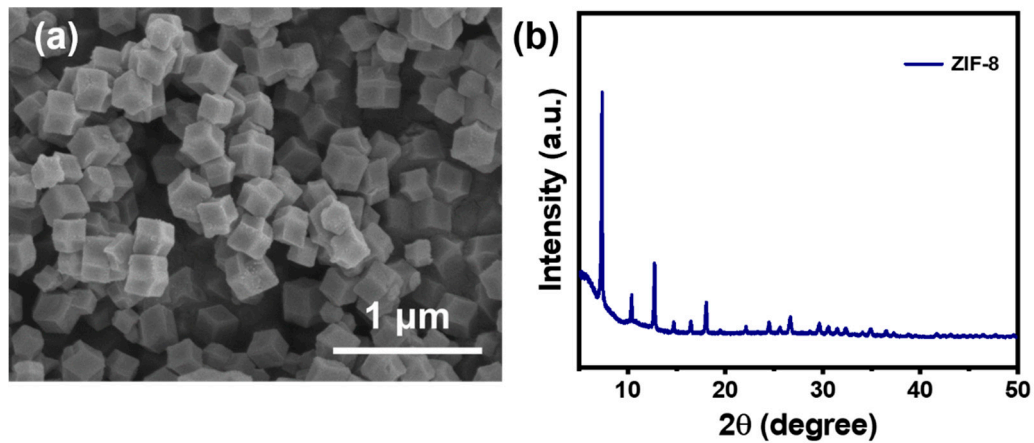


Figure S1. (a) SEM image and (b) XRD pattern of ZIF-8.

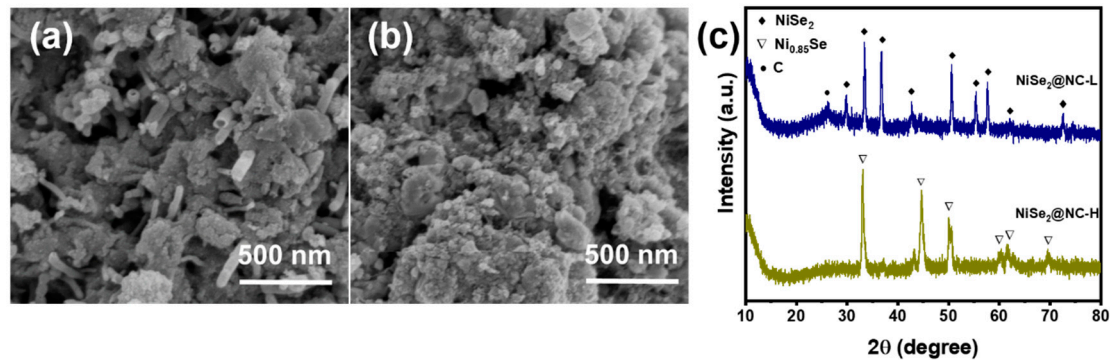


Figure S2. SEM images of (a) $\text{NiSe}_2@\text{NC-L}$ and (b) $\text{NiSe}_2@\text{NC-H}$. (c) XRD patterns of $\text{NiSe}_2@\text{NC-L}$ and $\text{NiSe}_2@\text{NC-H}$.

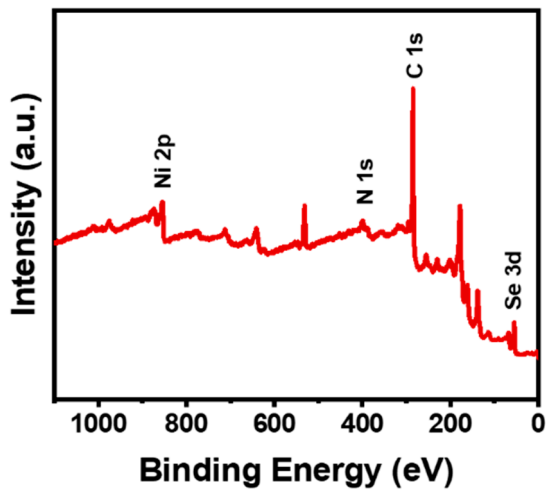


Figure S3. XPS full spectrum of NiSe₂@NC.

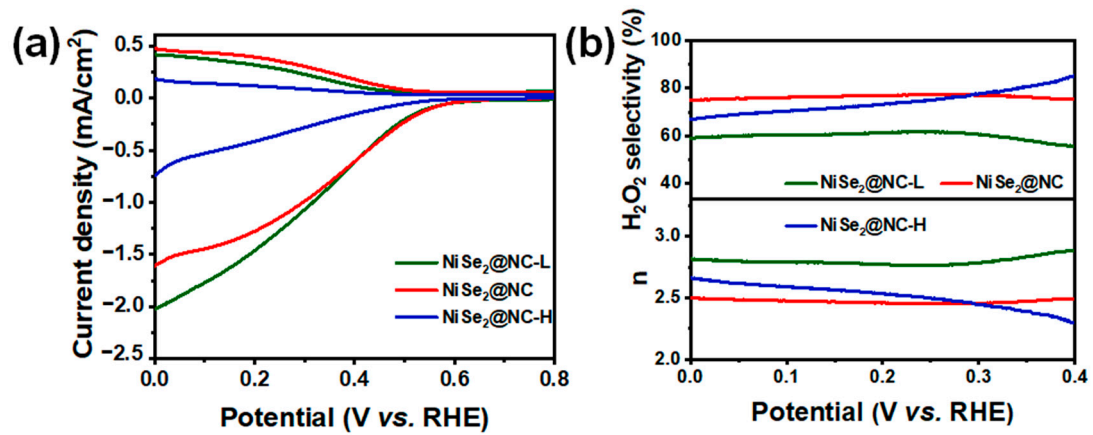


Figure S4. (a) RRDE polarization curves, (b) H_2O_2 selectivity and electron transfer number of $\text{NiSe}_2@\text{NC-L}$, $\text{NiSe}_2@\text{NC}$, and $\text{NiSe}_2@\text{NC-H}$ at 1600 rpm in O_2 -saturated 0.1 M HClO_4 .

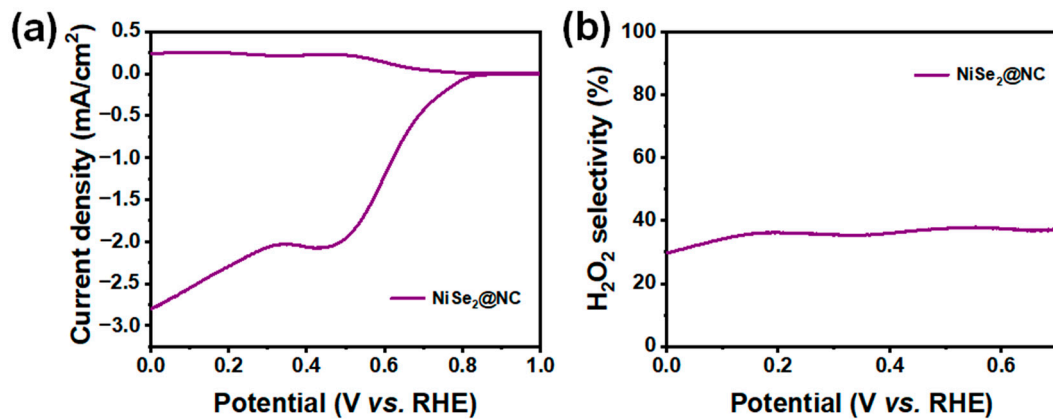


Figure S5. (a) RRDE polarization curves and (b) H_2O_2 selectivity of $\text{NiSe}_2@\text{NC}$ at 1600 rpm in O_2 -saturated 0.1 M KOH.

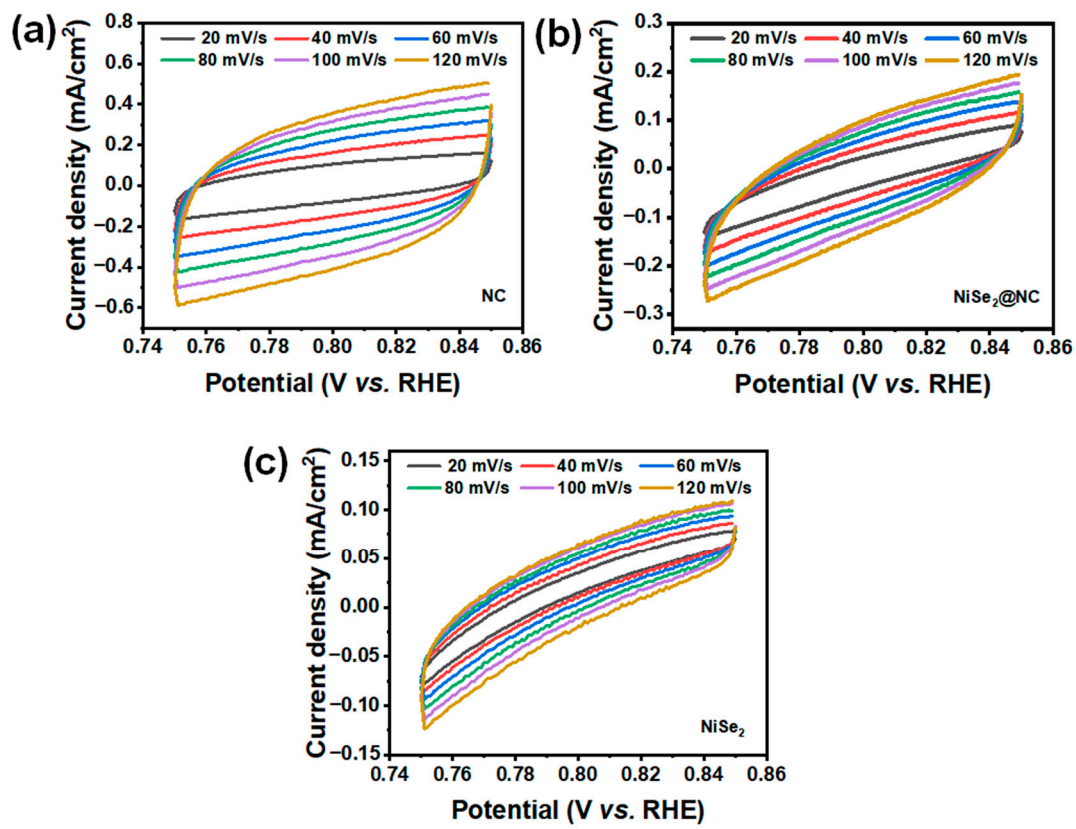


Figure S6. Cyclic voltammograms of (a) NC, (b) $\text{NiSe}_2@\text{NC}$, and (c) NiSe_2 at different scan rates.

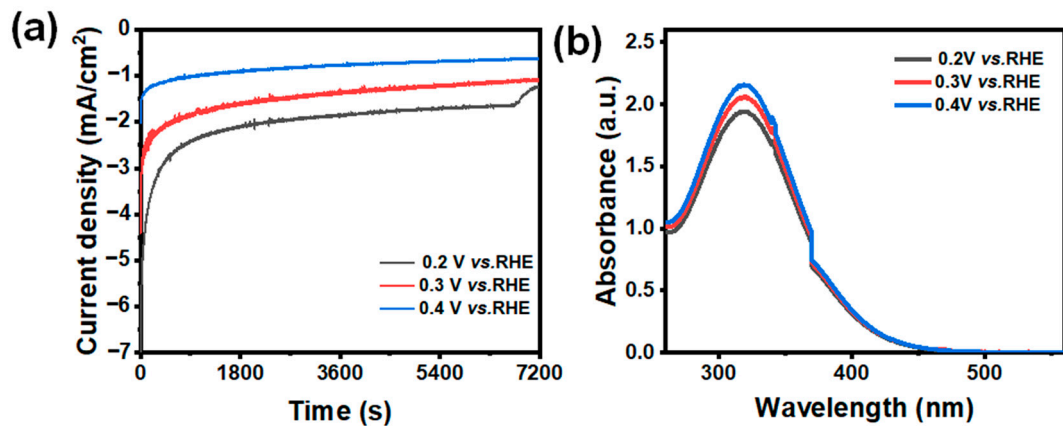


Figure S7. (a) Chronoamperometry curves for NiSe₂@NC at different potentials for 7200 s in O₂-saturated 0.1 M HClO₄ and (b) the corresponding UV-Vis spectra.

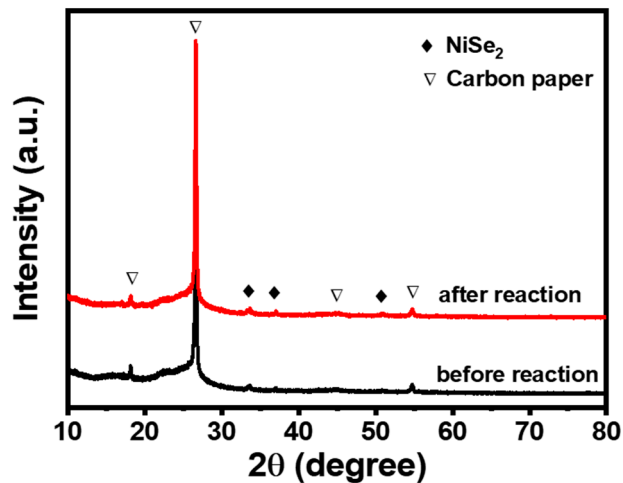


Figure S8. XRD patterns of NiSe₂@NC before and after electrolysis over the wide range.

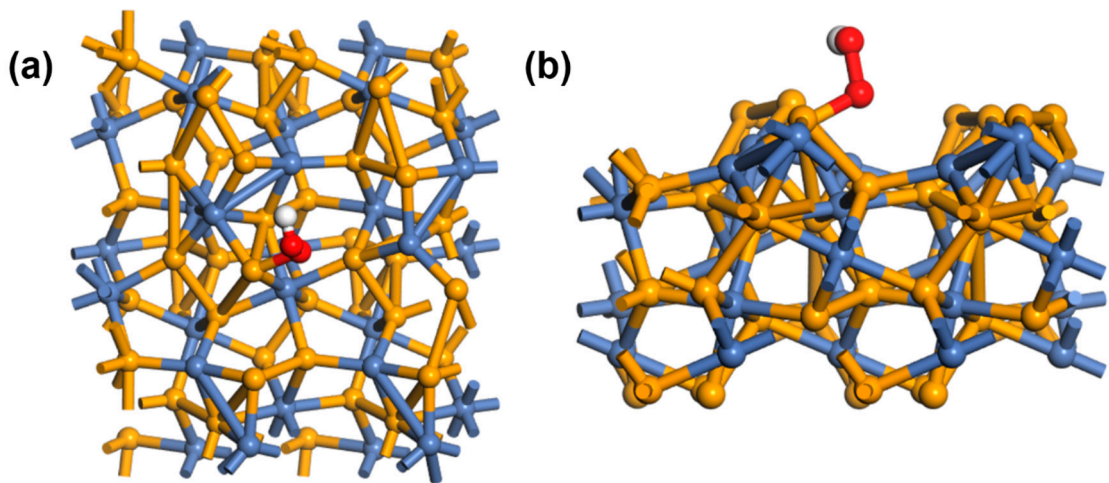


Figure S9. The DFT calculation models of NiSe₂-OOH, where the yellow, blue, red, and white spheres represent the Se, Ni, O, and H atom, respectively.

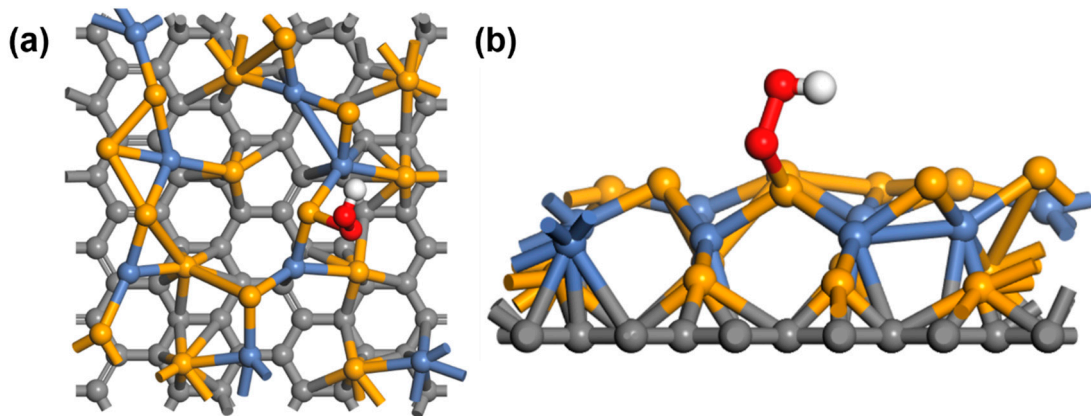


Figure S10. The DFT calculation models of NiSe₂@NC-OOH, where the yellow, blue, red, white, and grey spheres represent the Se, Ni, O, H, and C atom, respectively.

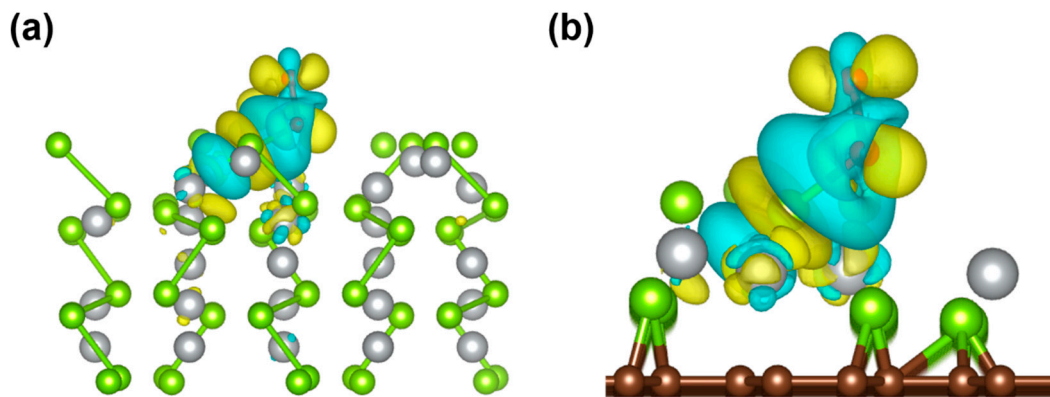


Figure S11. Differential charge density distributions between adsorbed *OOH and (a) NiSe₂ and (b) NiSe₂@NC substrates, where the green, grey, and brown sphere represent the Se and Ni atom, respectively, while the cyan and yellow color isosurface mean the negative and positive charge, respectively.

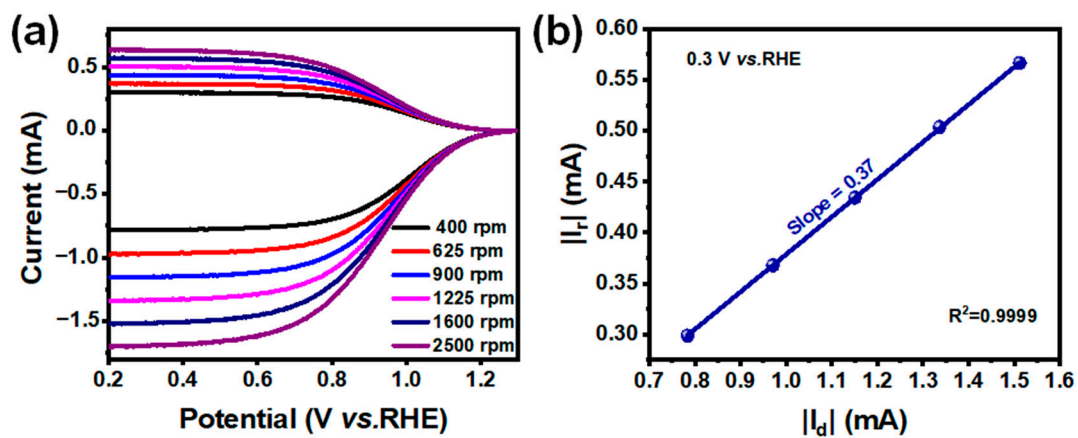


Figure S12. (a) LSV curves of RRDE at different speeds and (b) linear fitting curve of disk current and ring current.

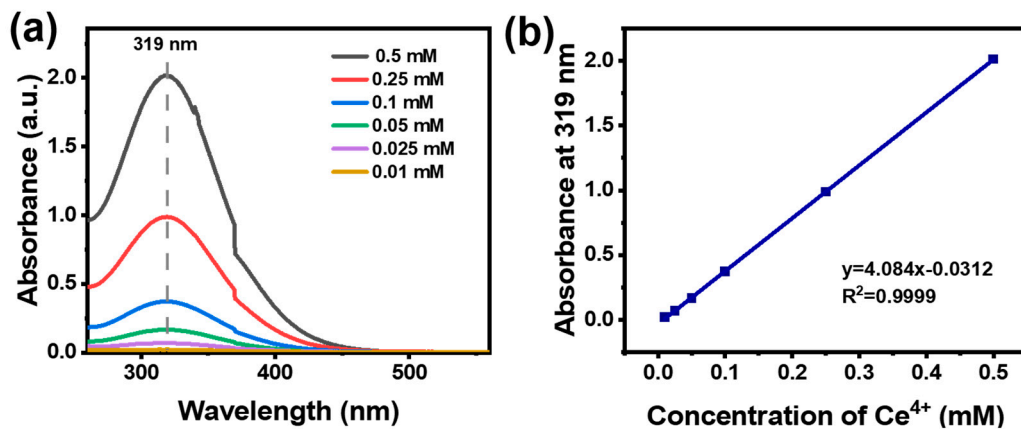


Figure S13. (a) UV-Vis spectra of different standard Ce^{4+} solution and (b) the corresponding standard curve.

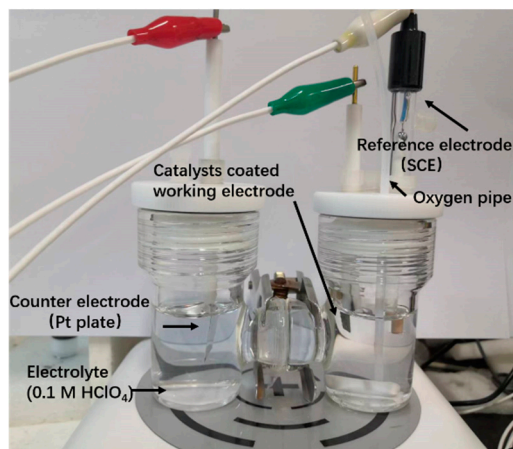


Figure S14. Diagram of H-type electrolytic cell reaction device.

Table S1. Comparison of 2e⁻ ORR properties with other transition metal chalcogenides.

Catalyst	Electrolyte	Maximum RRDE selectivity(%)	stability	Maximum FE (%)	Ref.
NiSe ₂ @NC	0.1 M HClO ₄	77	10 h	81	This work
CoS ₂	0.05 M H ₂ SO ₄	76	60 min	70	[1]
Co ₃ O ₄ -OVs/N-CNTs	0.5 M H ₂ SO ₄	67.6	5 h	56.1	[2]
NiSe ₂ -CP	0.05 M H ₂ SO ₄	88	12 h	90	[3]
CoTe@NC	0.1 M HClO ₄	92.6	12 h	—	[4]
CoSe ₂ @NCNTs	0.1 M HClO ₄	93.2	24 h	—	[5]
CuCo _{0.8} Ni _{1.2} S ₄	0.05 M H ₂ SO ₄	74	90 min	—	[6]
NiO	0.1 M KOH	79.4	—	—	[7]
CoPSe	0.1 M HClO ₄	85	10 h	85	[8]
CoSe ₂	0.5 M H ₂ SO ₄	> 90	5 h	91	[9]

References

- Sheng, H.; Hermes, E.D.; Yang, X.; Ying, D.; Janes, A.N.; Li, W.; Schmidt, J.R.; Jin, S. Electrocatalytic Production of H₂O₂ by Selective Oxygen Reduction Using Earth-Abundant Cobalt Pyrite (CoS₂). *ACS Catal.* **2019**, *9*, 8433-8442. <https://doi.org/10.1021/acscatal.9b02546>.
- Yan, L.; Cheng, X.; Wang, Y.; Wang, Z.; Zheng, L.; Yan, Y.; Lu, Y.; Sun, S.; Qiu, W.; Chen, G. Exsolved Co₃O₄ with tunable oxygen vacancies for electrocatalytic H₂O₂ production. *Mater. Today Energy* **2022**, *24*, 100931. <https://doi.org/10.1016/j.mtener.2021.100931>.
- Sun, Q.; Xu, G.; Xiong, B.; Chen, L.; Shi, J. Anion-tuned nickel chalcogenides electrocatalysts for efficient 2e⁻ ORR towards H₂O₂ production in acidic media. *Nano Res.* **2022**, *16*, 4729-4735. <https://doi.org/10.1007/s12274-022-5160-2>.
- Zhang, L.; Liang, J.; Yue, L.; Dong, K.; Xu, Z.; Li, T.; Liu, Q.; Luo, Y.; Liu, Y.; Gao, S.; et al. CoTe nanoparticle-embedded N-doped hollow carbon polyhedron: an efficient catalyst for H₂O₂ electrosynthesis in acidic media. *J. Mater. Chem. A* **2021**, *9*, 21703-21707. <https://doi.org/10.1039/d1ta06313h>.
- Zhang, L.; Liang, J.; Yue, L.; Xu, Z.; Dong, K.; Liu, Q.; Luo, Y.; Li, T.; Cheng, X.; Cui, G.; et al. N-doped carbon nanotubes supported CoSe₂ nanoparticles: A highly efficient and stable catalyst for H₂O₂ electrosynthesis in acidic media. *Nano Res.* **2021**, *15*, 304-309. <https://doi.org/10.1007/s12274-021-3474-0>.
- Ross, R.D.; Sheng, H.; Parihar, A.; Huang, J.; Jin, S. Compositionally Tuned Trimetallic Thiospinel Catalysts for Enhanced Electrosynthesis of Hydrogen Peroxide and Built-In Hydroxyl Radical Generation. *ACS Catal.* **2021**, *11*, 12643-12650. <https://doi.org/10.1021/acscatal.1c03349>.
- Zhang, Y.; Jiang, H.; Zhang, C.; Feng, Y.; Feng, H.; Zhu, S.; Hu, J. High-efficiency oxygen reduction by late transition metal oxides to produce H₂O₂. *J. Mater. Chem. A* **2024**, *12*, 6123-6133. <https://doi.org/10.1039/d3ta06995h>.

8. Xie, J.; Zhong, L.; Yang, X.; He, D.; Lin, K.; Chen, X.; Wang, H.; Gan, S.; Niu, L. Phosphorous and selenium tuning Co-based non-precious catalysts for electrosynthesis of H₂O₂ in acidic media. *Chin. Chem. Lett.* **2024**, *35*, 108472. <https://doi.org/10.1016/j.cclet.2023.108472>.
9. Zheng, Y.R.; Hu, S.; Zhang, X.L.; Ju, H.; Wang, Z.; Tan, P.J.; Wu, R.; Gao, F.Y.; Zhuang, T.; Zheng, X.; et al. Black Phosphorous Mediates Surface Charge Redistribution of CoSe₂ for Electrochemical H₂O₂ Production in Acidic Electrolytes. *Adv. Mater.* **2022**, *34*, 2205414. <https://doi.org/10.1002/adma.202205414>.